Available online at www.sciencedirect.com
SCIENCE DIRECT®
International Journal of Mass Spectrometry 228 (2003) 687–702
International Journal of Mass Spectrometry
www.elsevier.com/locate/ijms

Neutralization–reionization of ions produced by electrospray Instrument design and initial data

Jennifer L. Seymour, Erik A. Syrstad, Charley C. Langley, František Tureček*

Department of Chemistry, Bagley Hall, Box 351700, University of Washington, Seattle, WA 98195-1700, USA

Received 18 December 2002; accepted 21 March 2003

Dedicated to Professor Helmut Schwarz on the occasion of his 60th birthday.

Abstract

A tandem mass spectrometer is described for neutralization–reionization studies of ions produced by electrospray ionization. The instrument consists of a high current electrospray source, an electrodynamic ion funnel, and an octopole ion guide that transport the ions into the high vacuum region of the tandem mass spectrometer. The ions are accelerated to 8250 eV and submitted to collisional neutralization and reionization, followed by deceleration, separation by kinetic energy and/or mass, and detection. The performance of the ionizer and ion transfer elements is optimized as a function of background pressure and the applied rf and dc potentials. Examples are given for neutralization–reionization mass spectra of protonated adenine, heterocycles, and β-alanine-*N*-methyl amide.

Keywords: Neutralization–reionization; Electrospray interface; Adenine radical; Heterocyclic radicals; Amino acid radicals

1. Introduction

Electrospray ionization (ESI) [1] is a soft ionization method that achieves ion transition from solution to the gas phase. In addition to being used in numerous applications to biomolecule analysis [2], ESI has also served to produce various ion species that have been investigated by the methods of gas-phase ion chemistry. There are a few examples of using ESI in coupling with special mass spectrometric techniques that probe ion structure and energetics, such as flowing afterglow [3,4], photoelectron spectroscopy [5], and ion mobility mass spectrometry [6].

Neutralization–reionization mass spectrometry (NRMS) is a method that has been used for both ion characterization and the generation of a variety of transient neutral intermediates and elusive molecules in the gas phase, as reviewed [7–14]. When applied to cations, NRMS utilizes collisional electron transfer from a suitable donor (gaseous thermal atom or molecule) to a fast ion that has been accelerated to 5–10 keV kinetic energy and is traveling at a 100,000–200,000 m/s velocity. As follows from the collision kinematics, electron transfer is confined to typically occur within 1–10 fs so that the nascent neutral species are formed with the structure of the precursor ion. Likewise, fast anions can be converted to neutral intermediates by collisional electron detachment [15] or laser photodetachment [16]. Fast transient

* Corresponding author. Tel.: +1-206-685-2041; fax: +1-206-685-3478.
E-mail address: turecek@chem.washington.edu (F. Tureček).

1387-3806/$ – see front matter © 2003 Elsevier Science B.V. All rights reserved.
doi:10.1016/S1387-3806(03)00217-3

neutral intermediates produced by either method can be interrogated by collisional activation [17], laser photoexcitation [18], or by determining unimolecular rate parameters by the variable-time method [19]. Detection is achieved following non-selective collisional ionization [20] and mass spectrometric analysis. Neutralization–reionization mass spectra can be obtained for all four combinations of cations and anions, e.g., cation → neutral → cation ($^{+}NR^{+}$), anion → neutral → cation ($^{-}NR^{+}$), etc. [15].

Applications of NRMS critically depend on our ability to generate precursor ions in the gas phase. For small molecular systems, precursor ions can often be formed by dissociative ionization or ion–molecule reactions using volatile compounds. These gas-phase ionization methods hinge on the knowledge of gas-phase ion chemistry and sometimes allow one to roughly control ion internal energies by choosing an appropriate energy regime for dissociative ionization, e.g., by lowering the electron energy or using metastable ion precursors. Likewise, energy control in ion–molecule reactions can be achieved by choosing a reactant ion of an appropriate recombination energy for charge-exchange ionization, or an appropriate gas-phase acid or base in proton transfer reactions. Nevertheless, generation of fully thermalized ions is problematic, and temperature control is awkward and limited to be within the usual ion source temperature regime (423–523 K). Another limitation inherent to gas-phase ionization methods is caused by the absence of solvent, which affects the precursor compound acidity and basicity, and can lead to different protonation sites in solution and the gas phase. The limitation due to compound volatility can be in part offset by using fast-atom bombardment ionization [21,22] which, however, suffers from limited sample duration and lack of control of ion internal energies.

It appears that out of the currently available soft ionization methods, ESI has all the desired qualities in generating continuous high ion currents of ions with internal energies close to thermal equilibrium [23]. In this paper, we describe a new ESI source and transfer ion optics that has been coupled to a tandem quadrupole acceleration–deceleration mass spectrometer [24] for NRMS studies of involatile molecules.

2. Ion source and interface design

The following description of the instrumental design will focus on the construction of the electrospray source and interface for ion transfer from atmospheric pressure to the high vacuum region, as the remaining portion of the instrument has been previously documented and used without further modification [24]. Fig. 1 is an overall schematic representation of the new ESI source. Description of the instrumental design can be separated into three distinct regions, based upon pressure regimes of the instrument, i.e.: (1) atmospheric pressure region, (2) roots-pumped low vacuum region, and (3) diffusion-pumped high vacuum region.

2.1. Atmospheric pressure region

The electrospray needle is made from 100 mm long stainless steel tubing (1.59 mm (1/16 in.) o.d., 0.25 mm i.d.) that was tapered at a 20° angle by grinding to a point. The needle is mounted on an XYZ translator (Edmund Industrial Optics, Barrington, NJ) to allow for adjustment of the needle position. The angle of the needle can be adjusted and is usually operated at approximately 30° above the optical axis of the instrument. A dc potential is applied to the needle from a 5 kV/3 mA high voltage power supply (Bertan, Vallhala, NY) and usually ranges between 2.0 and 4.0 kV. Sample is directly infused into the mass spectrometer by a syringe pump (KD Scientific, New Hope, PA) through 1.59 mm o.d., 0.15 mm i.d. PEEK tubing at a flow rate of between 1.0 and 4.0 μl/min.

The needle is manipulated to focus the spray through a 6.35 mm (1/4 in.) aperture in the outer faceplate of the source. The faceplate is an aluminum cylinder, 93 mm in diameter and 35 mm tall, containing an electrical interface to supply power to the heater block, and an air inlet for the introduction of nitrogen as a drying gas. A dc potential is applied to

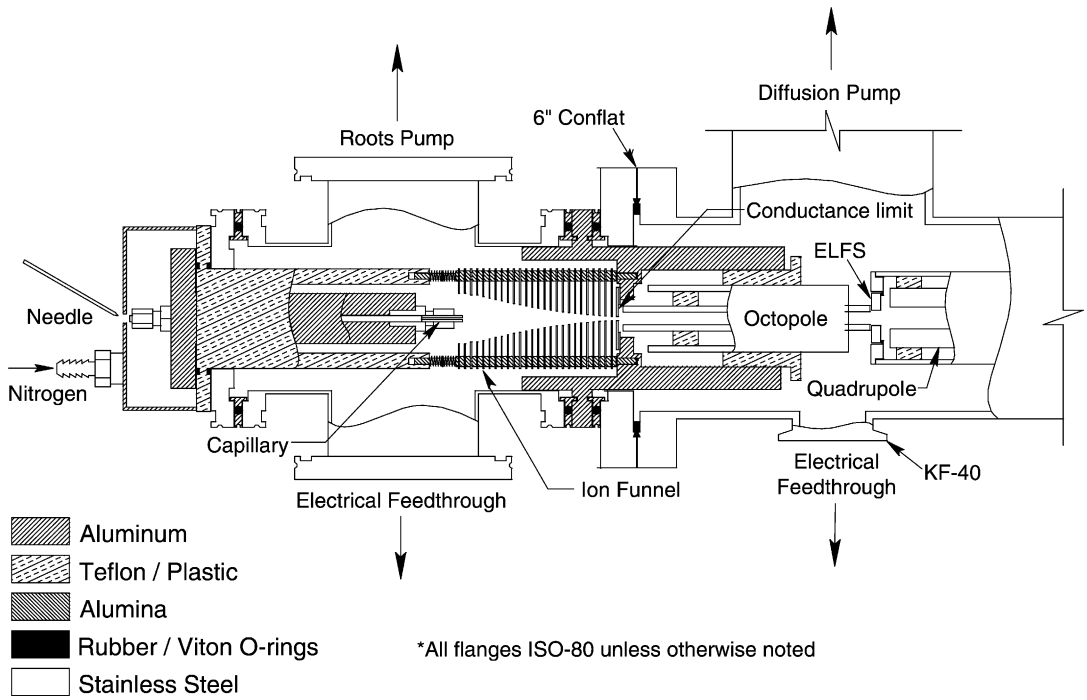

Fig. 1. Schematic drawing of the electrospray ionizer, ion transfer elements, and vacuum housing.

the faceplate from a 3 kV/5 mA high voltage power supply (Bertan, Valhalla, NY). The normal operating range for the faceplate potential is between 200 and 400 V dc. Directly behind the aperture drilled in the faceplate is a glass-lined stainless steel transfer capillary (170 mm length, 3.2 mm o.d., 1.0 mm i.d.) and the heater block.

The aluminum heater block is held at the same dc potential as the faceplate of the ESI by using 3.2 mm metal Swagelok fittings that hold the transfer capillary into the block. The heater block is 124 mm long, with an initial diameter of 70.6 mm for the first 12.7 mm, then this decreases to 25.4 mm for the rest of the length of the block. The block contains two drilled holes, one for a 6.35 mm 120 V 80 W 25.4 mm long cartridge heater, and the other for a type K thermocouple to monitor the temperature of the heater block. The heater block and faceplate are insulated from the instrument by a Teflon liner that rests underneath the wider portion of the heater block and extends back into the first pumped region of the instrument. The Teflon liner is 118 mm long, with an initial diameter of 94 mm, but after 7 mm the diameter decreases to 34.8 mm in order to fit inside the vacuum system. The heater block is attached to the Teflon liner by six 4–40 screws and a 50.47 mm i.d. Viton O-Ring. The Teflon liner by use of another 50.47 mm i.d. Viton O-Ring is fitted to an ISO 80 flange that has been bored to an i.d. of 34.8 mm, allowing the liner to pass into the six-way cross and the roots-pumped region.

2.2. Low vacuum region

The vacuum housing is a six-way cross that is pumped by a Leybold WA501/D65B roots pump (Cologne, Germany) which, when operating with the 1.0 mm i.d. transfer capillary, produces an average pressure of 0.60 Torr in this region. When operating with a smaller capillary i.d., for example, 0.8 mm i.d., the pressure is approximately 0.34 Torr. The pressure in this region is monitored by a 345 Shielded Pirani Vacuum Gauge (MKS Instruments, Andover, MA)

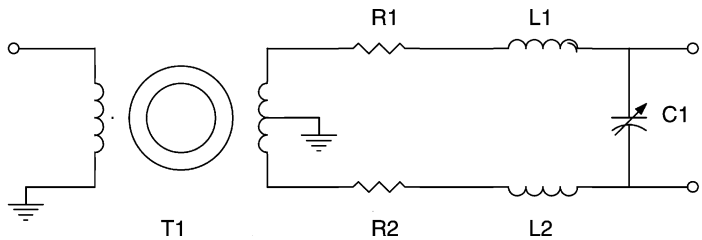

Fig. 2. Phase splitting circuit for the ion funnel. T1 is the transformer, R1 and R2 are 28 and 8 W resistors, L1 and L2 are 42 mH inductors, and C1 is a 45–1000 pF air variable capacitor.

and attached to the six-way cross via an ISO 80 to KF 25 adaptor. Power and radio frequency (rf) are supplied to the six-way cross by a 10-pin KF 50 electrical feedthrough (MDC, Hayward, CA) connected by an ISO 80 to KF 50 adaptor.

The transfer capillary exits into the six-way cross, directly into an electrodynamic ion funnel which focuses the ions leaving the transfer capillary. The design of the ion funnel is based upon the work of Shaffer et al. [25a–c]. The funnel is spring mounted into the Teflon liner to ensure a tight fit up against the next region of the instrument and to ensure consistent mounting in alignment with the conductance limit. The ion funnel consists of twenty-six 35.56 mm square, 0.635 mm thick stainless steel ring electrode plates with sequentially decreasing apertures (25.4–2 mm). The plates are mounted on four alumina rods and separated by 2.54 mm alumina spacers. The plates are connected through a resistor chain of 9.2 MΩ resistors, to produce a dc gradient. A dc potential, split from the same power source as the faceplate and capillary, is applied to the first plate of the ion funnel, so that all three components are held at the same potential. The potential on the last plate in the ion funnel is controlled separately by tapping one of the dc voltages provided by an Extrel C-50 power supply (ABB, Pittsburgh, PA) to define the dc potential gradient.

The rf signal applied to the ion funnel elements is produced by a wave-form generator (model 72-5010 Tenma, Springborn, OH) and amplified using a broad-band rf amplifier (model 350L, ENI, Rochester, NY). The unbalanced input from the rf amplifier is split into two signals of equal magnitude and opposite phase using the circuit shown in Fig. 2 and is then applied to alternating elements of the ion funnel. No amplitude loss occurs across the phase splitter circuit (Q factor is equal to 1). This balun transformer (T1) consists of a toroidal ferrite core (CWS, Santa Ana, CA) with 30 turns of 16-gauge magnet wire (Radar Electric, Seattle, WA) for the primary coil and 21 turns of 14-gauge magnet wire (Radar) for each of the secondary coils. The two secondary coils are produced by center tapping a 42-coil winding. The 28 Ω 8 W resistors (R1, R2) are composed of four 110 Ω (5%) 2 W resistors in parallel. The 42 μH conductors (L1, L2) are made using 7 turns of 16-gauge magnet wire (Radar) around a toroidial ferrite core (CWS). The 45–1000 pF air variable capacitor (C1) (Surplus Sales of Nebraska) is used to tune the resonance of the complete ion funnel circuit. The resonant frequency for the ion funnel circuit using the head was 800 kHz. Normal operational settings of the ion funnel rf generator range between 700 kHz and 2.0 MHz, 100–150 V peak-to-peak voltage (V_{pp}), and vary with properties of the analyte, such as molecular weight and structure. The two phases of the rf signal are applied to alternating plates on the ion funnel and are capacitively decoupled from the dc potential by 1 kV/47 pF capacitors. A 2.0 mm aperture that serves as both the conductance limit for the following region of pumping and another extraction lens is located 1.4 mm from the last plate of the ion funnel. The voltage on the conductance limit can be independently tuned from the Extrel C-50 dc power supply (vide supra).

A stainless steel sleeve was designed to provide the connection to the next vacuum region. The sleeve

is 133 mm long, with 48.1 mm extending into the six-way cross to hold the ion funnel in alignment with the conductance limit. The inner diameter of the ion funnel side of the sleeve is 59.2 mm with a section machined out to a diameter of 67.3 mm to accommodate the rather bulky capacitor chain. The sleeve has two ISO 80 mating surfaces, one that connects to the ion funnel side of the instrument, and one that connects back towards the next region of pumping. This second side of the sleeve has an i.d. of 49.0 mm and extends into the existing instrument.

The vacuum housing of the ESI source was built using ISO flanges, but the tandem quadrupole instrument has a 6 in. conflat flange as the front port. Therefore, in order to make transition from the new ESI source to the tandem instrument, a custom adaptor flange was designed. This flange was constructed from a blank 6 in. conflat that was bored to a 73.66 mm i.d., and one side of the flange was machined to fit an ISO 80 centering ring with an o.d. of 83.31 mm. The flange is held in place by machined clamps and four 76.2 mm long, brass-plated stainless steel Grade 6 bolts successfully mating the ISO flange to the 6 in. conflat.

2.3. High vacuum region

The second differentially pumped region in the instrument uses the existing 1200 L/s diffusion pump (Varian VHS-4; Varian Associates, Lexington, MA); this region is usually operated at pressures ranging from 4.5×10^{-4} to 7.0×10^{-4} Torr. This region houses the octopole ion guide. The stainless steel octopole rods are 127 mm long with 3.175 mm diameter and an inscribed diameter of 6.35 mm. The octopole is insulated from its stainless steel casing by a Teflon mounting. The casing is 101.6 mm long and centered on the octopole, so that the rods extend out of the casing by 12.7 mm on either side. This casing is held into the stainless steel sleeve by two Teflon clamps that allow the position of the octopole to be adjusted along the optical axis of the instrument. The octopole is floated at a dc potential, ~65 V, from the Extrel C-50 power supply. The rf signal is generated using a Tenma wave-form generator (model 72-5010) and is amplified using a 150 W broad-band rf amplifier (model 2100L, ENI). The rf signal is split using the circuit shown in Fig. 3. The 30 Ω 8 W resistors (R3, R4) are composed of four 120 Ω 2 W (10%) resistors in parallel. The 85 μH inductors (L3, L4) have toroidal ferrite cores (CWS) with 10 turns of 16-gauge magnet wire (Radar). The transformer (T2) contains a 15-turn (14-gauge) magnetic wire primary coil with a 50-turn secondary coil (16-gauge) center tapped to produce two 25-turn secondary coils. Resonant frequency of the octopole-head circuit is 1.2 MHz. The ground for the secondary coil, resistors, and inductors of the octopole phase splitter is equal to the float voltage of the octopole.

The normal operational frequency range for the octopole is between 1.0 and 2.0 MHz, and an amplitude of 100–200 V (V_{pp}). Both rf and dc potentials are fed into the instrument through a 10-pin KF 40 electrical feedthrough, (Lesker, Clariton, PA). Through this feedthrough, the Extrel C-50 power supply is also connected to the lens that injects ions into the first quadrupole mass filter (ELFS lens), which is floated slightly lower than the octopole to extract the ions into quadrupole I of the tandem instrument. The ELFS lens

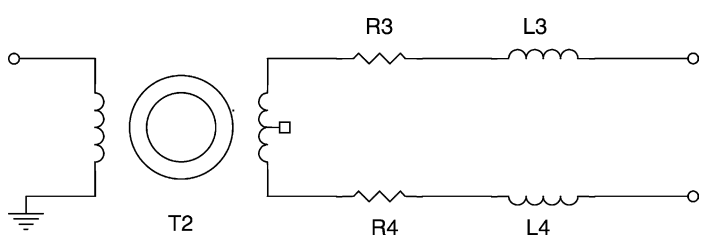

Fig. 3. Q-head for the octopole ion guide. The abbreviations are as in Fig. 2.

was modified by removing the ferrite core in order to increase the diameter of the aperture, allowing for increased ion transmission.

3. Ion transmission characteristics

Neutralization–reionization results in substantial ion losses that are caused by low efficiency of the neutralization (1–10% conversion efficiency) and reionization (0.1–0.5% conversion efficiency) steps and further aggravated by imperfect ion transmission through the mass analyzers. Scheme 1 shows the typical ion transmissions in the tandem quadrupole mass spectrometer obtained for precursor ion transport through quadrupole I in the rf-only mode, neutralization, reionization, and product ion mass separation at unit mass resolution in quadrupole II [24].

Therefore, it is important that any ion source coupled to the instrument provide substantial current to produce a detectable signal after neutralization and reionization collisions. The ion funnel designed for this instrument took into consideration the design alterations suggested by Tolmachev et. al. [26] and Lynn et. al. [27] in their extensive computer simulations modeling the performance of the ion funnel. Therefore, several experiments were conducted to compare the performance of this ion funnel to those simulations.

The ion current was usually monitored at the final detector after quadrupole II to determine which variables in the source would affect the intensity of the current. Although these measurements do not provide absolute ion currents, they allow the ESI interface tuning parameters to be conveniently monitored and optimized. Ion transmission through quadrupole I, quadrupole II, and the electrostatic lenses has been measured previously [24] and was assumed to be the same after the ESI source was added. Alternatively, total ion current was monitored at a stainless steel collector plate that was placed to cover the entrance to quadrupole I. The total mass-unresolved ion current in this region was in the 1–2 nA range, corresponding to the fraction of ESI ions transmitted by the funnel lens and the octopole.

A 100 μM solution of 2,2′-bipyridine with 0.05% acetic acid (Aldrich, Milwaukee, WI) was electrosprayed and the mass-analyzed current of the ion of protonated 2,2′-bipyridine, $[bpy + H]^+$, was used to determine the relative ion transmission characteristics of the ion funnel and octopole. Other molecules, adenine, β-alanine-*N*-methyl amide, crystal violet, and 1,10-phenanthroline (Aldrich, Milwaukee, WI), were also electrosprayed to determine the effect that various *m*/*z* and compound structures had upon the performance of the ion funnel and octopole. Fig. 4 shows the $[bpy + H]^+$ ion intensity as a function of the rf (Fig. 4a) and amplitude (Fig. 4b) applied to the ion funnel at varying pressures in the low vacuum region. Different pressures were achieved by choking off the gate valve that separates the roots pump from the six-way cross. The $[bpy + H]^+$ ion intensity showed a definite maximum as the frequency of the ion funnel rf signal was adjusted, suggesting that the frequency be tuned for the analyte under observation, as a set frequency may not be the correct ion transmission window. Fig. 4a also shows that the intensity of $[bpy + H]^+$ at a given frequency depends on the background gas pressure in the region, showing similar behavior to that modeled by Lynn et. al. [27] for the various charge states of cytochrome *c* ions. However, the data of Lynn et al. suggest that it is the charge

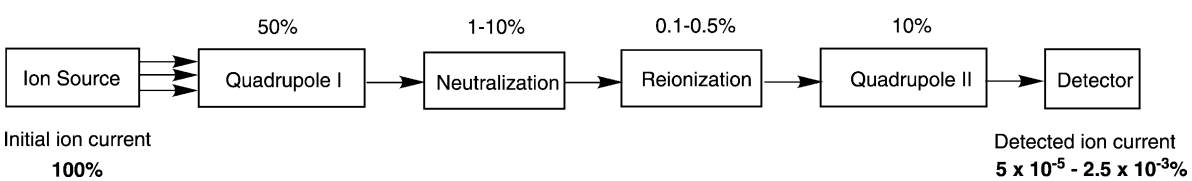

Scheme 1.

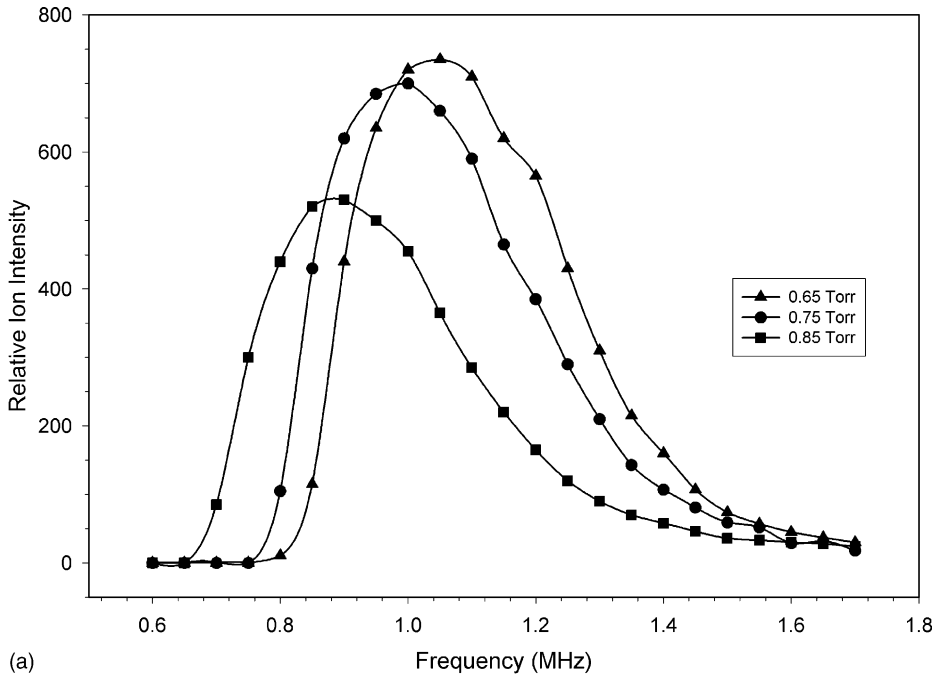

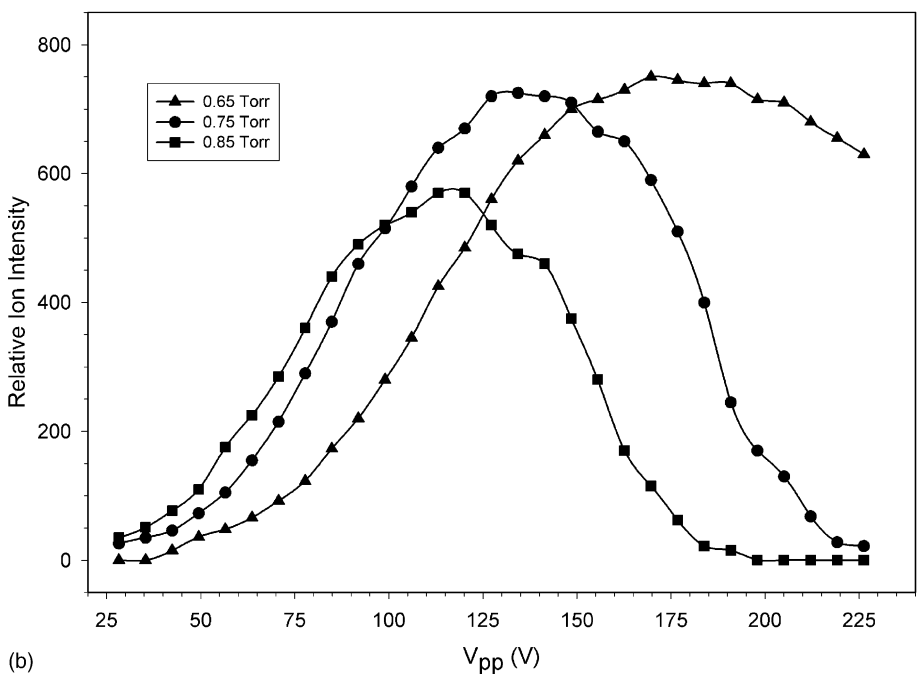

Fig. 4. Ion intensity for $[bpy + H]^+$ plotted as a function of ion funnel (a) radio frequency and (b) amplitude (V_{pp}).

state that is responsible for shifting the intensity maxima, whereas our data suggest that the pressure regime can shift the maximum within the same *m*/*z*. It has been found that optimal experimental pressures for this region are approximately 0.35–0.80 Torr for organic molecules of molecular mass greater than 100 Da. Pressures greater than 1 Torr cannot presently be achieved with this design of the instrument, as the gas load on the second pumped region is too great for the current diffusion pump. Fig. 4b shows that the ion current depends on the amplitude of the rf signal (V_{pp}) applied to the ion funnel at different pressures. The maximum ion current intensity for $[bpy + H]^+$ was obtained at 170 V (V_{pp}), 0.65 Torr, and 1.05 MHz.

Three different octopoles were designed with different inscribed diameters, e.g., octopole I (8.56 mm i.d.), octopole II (6.35 mm i.d.), and octopole III (4.76 mm i.d.). Each of the octopoles was mounted in the instrument, and experiments were conducted to determine which octopole geometry allowed the greatest ion transmission. The intensity of several different analytes was again measured at the final detector. In Table 1, the ratio of the intensity of a given analyte to the highest intensity that has been experimentally observed is used to determine the best octopole for this instrument. The detector monitors the intensity in arbitrary units so to compare values among analytes, the highest intensity reading which was for Cs^+ (*m*/*z* 133) from CsCl on octopole II was used as a comparison to all other values. Intensity readings of other analytes, obtained with the same high voltage applied to the electron multiplier (−1.40 kV), were divided by this value to show a ratio of [analyte]/[CsCl, octopole II]. Generally, the intensity ratios were higher with octopole II, and this was chosen to be the octopole used for further experiments.

The octopole is located in a region where pumping is provided by the 1200 L/s diffusion pump, which is kept fully open for all experiments. The ion intensity was plotted against the rf and amplitude applied to the octopole at a constant pressure of 5.4×10^{-4} Torr. In Fig. 5a, the rf of the octopole was varied, while the amplitude was held constant at 76 V (V_{pp}). This experiment demonstrated a frequency plateau for 2,2′-bipyridine; however, below 1.5 MHz the signal dropped sharply, showing that the octopole is robust at higher frequencies, but should be tuned for each compound to determine the correct plateau range. Caution needs to be exercised with the frequency measurements, as adjusting the variable capacitor affects the response of the Q-head and the circuit resonance frequency. Fig. 5b shows the ion current dependence on the rf amplitude at the constant frequency of 1.69 MHz. These data are very similar

Table 1
Relative ion currents transmitted through octopole ion guides

Compound	*m*/*z*	Relative ion intensity[a]		
		Octopole I[b]	Octopole II[c]	Octopole III[d]
CsCl	133	0.21	1.00	–[e]
Adenine	136	–	0.71	0.50
2,2′-Bipyridine	157	0.14	0.68	0.43
1,10-Phenanthroline	181	–	0.64	–
[Cu(Ile − H)bpy]	349	–	0.11	0.003
Crystal violet	372	0.21	0.20	0.18

[a] Ratio of ion intensity, [analyte]/[highest current observed], for three octopoles of varying inscribed diameter to determine optimal ion transmission performance. The ratio was calculated by dividing the intensity of the analyte ion by the highest intensity observed (Cs^+ from CsCl, octopole II).
[b] 8.56 mm inscribed diameter.
[c] 6.35 mm inscribed diameter.
[d] 4.76 mm inscribed diameter.
[e] Not measured.

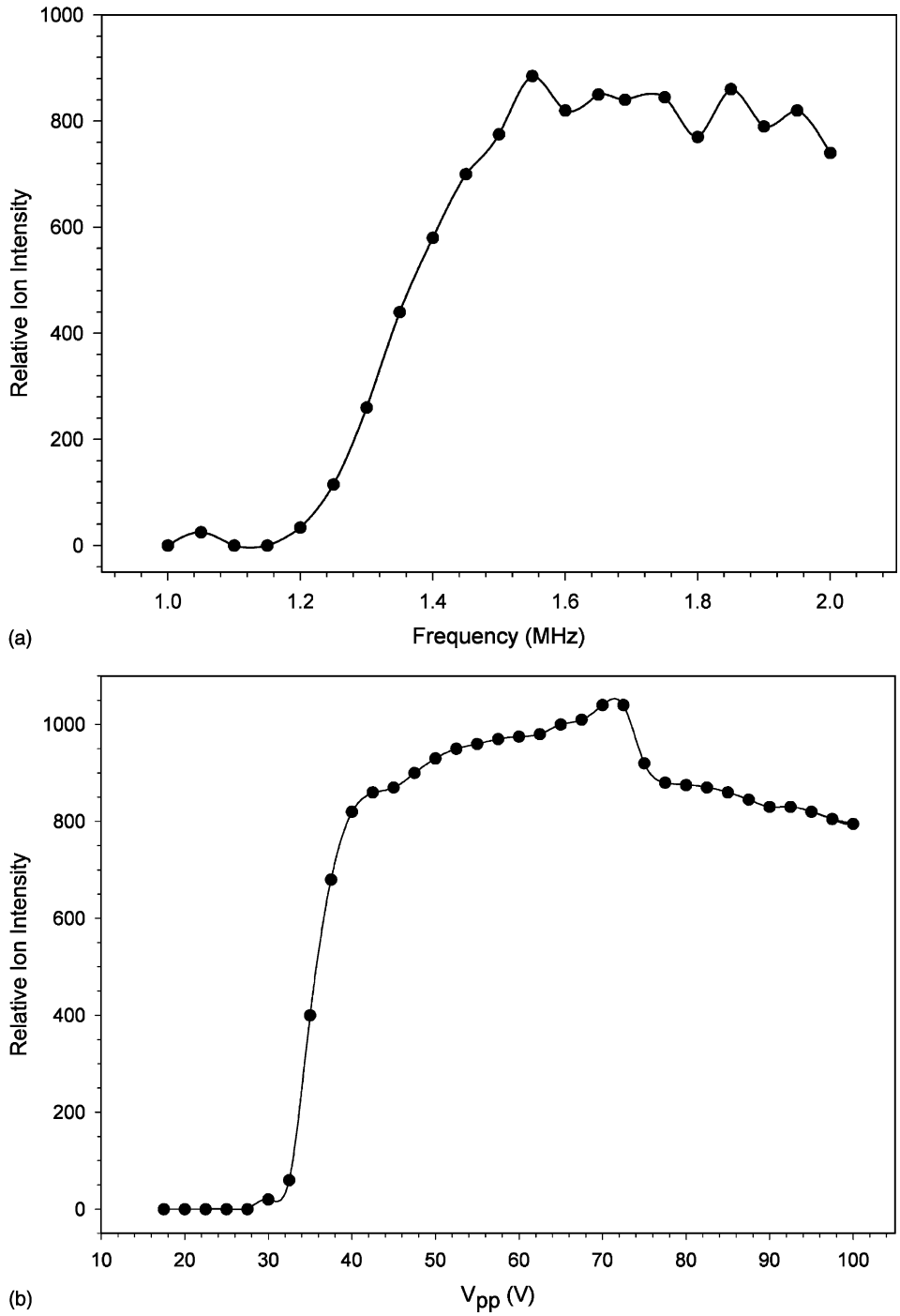

Fig. 5. Ion intensity for $[bpy + H]^+$ plotted as a function of octopole (a) radio frequency and (b) amplitude(V_{pp}).

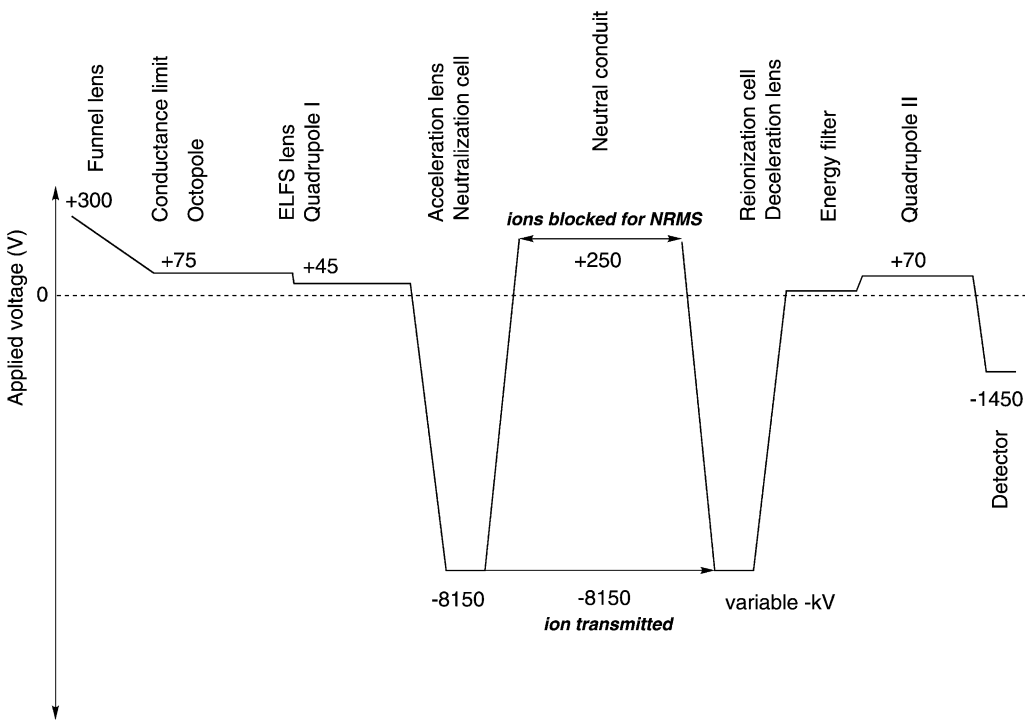

Fig. 6. Electrostatic potential profile along the ion path in the ESI-NR tandem mass spectrometer.

to that reported in Tolmachev et al.'s simulations, showing a steep increase to a flat region of stability. Unlike the simulations, we have observed that as the rf amplitude is further increased, the ion intensity decreased, providing a broad operational maximum.

The ions transmitted through the tandem instrument undergo several changes in kinetic energy due to acceleration and deceleration potentials (Fig. 6). Because transmission through the chicane-lens energy filter [24] decreases sharply at ion kinetic energies <40 eV, the instrument is typically operated with initial ion kinetic energies of 75–80 eV. This mandates that the ions be injected into the high vacuum region with kinetic energies >40 eV and preferably close to 80 eV. This requirement is met by floating the last element of the ion funnel lens, the conductance limit aperture, the octopole, and the injection ELFS lens at 70–75 V. Thus, while the ions undergo collisional cooling in the low vacuum regions, they gain the required kinetic energy when passing from the octopole to quadrupole I where the low pressure allows them to maintain the hyperthermal kinetic energy because of a sufficiently long mean free path. Further four-stage differential pumping in the high vacuum region secures that the ion and neutral kinetic energies are not substantially affected by collisions with the background gas. The neutralization and reionization collision cells are operated at pressures that favor single-collision conditions.

4. Neutralization–reionization mass spectra

In all NRMS measurements, ESI produced cations were transported to the high vacuum region by quadrupole I that was operated in an rf-only mode, accelerated to 8250 eV, and neutralized by collisions with dimethyl disulfide at 70% ion beam transmittance (T). Following collisional reionization with O_2 (70% T), the products were analyzed by kinetic energy only

or by mass and kinetic energy. The kinetic energy-only analysis provides four- to fivefold higher transmission of reionized species resulting in better signal-to-noise ratios in the spectra, but typically achieves low mass resolution and may involve artifact peaks arising from contaminants in the precursor ion beam. Fig. 7a shows the ESI mass spectrum of the nucleobase adenine which contains mostly the peak of protonated adenine

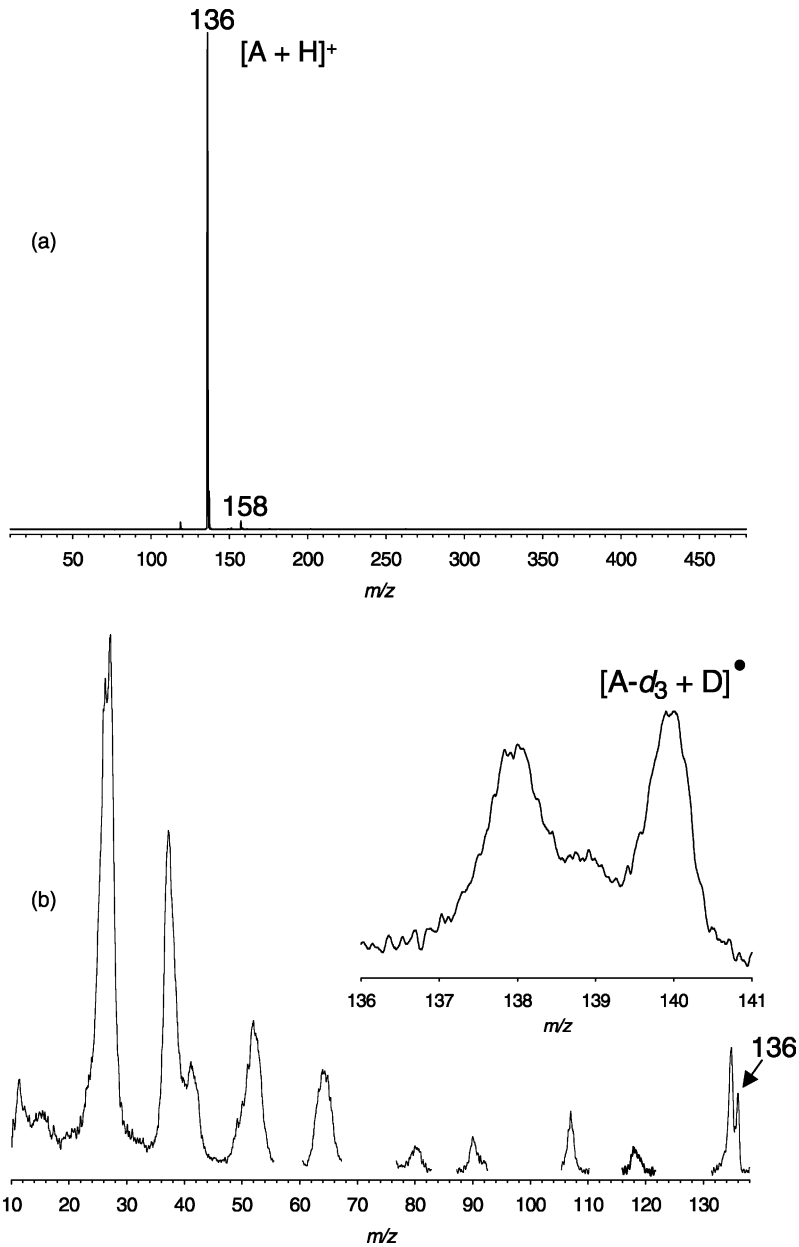

Fig. 7. (a) ESI mass spectrum of adenine. (b) $^{+}NR^{+}$ mass spectrum of [adenine + H]$^{+}$obtained as a kinetic energy scan. The inset shows the survivor ion region in the $^{+}NR^{+}$ mass spectrum of [adenine-d_3 + D]$^{+}$.

$[A + H]^+$ at *m*/*z* 136 (100%). Minor peaks appear at *m*/*z* 158 corresponding to $[A + Na]^+$ (1.5%) and *m*/*z* 119 corresponding to $[A + H - NH_3]^+$ (1.3%). $^+NR^+$ of this mixture, obtained by a ion kinetic energy scan, yields the spectrum shown in Fig. 7b. This shows a substantial survivor ion at *m*/*z* 136, and fragments at *m*/*z* 135 (loss of H), 118 (loss of $H + NH_3$), 107 (loss of C, N, H_3), 91, 90, 80, 64, 52, 42 (C_2H_4N), 38

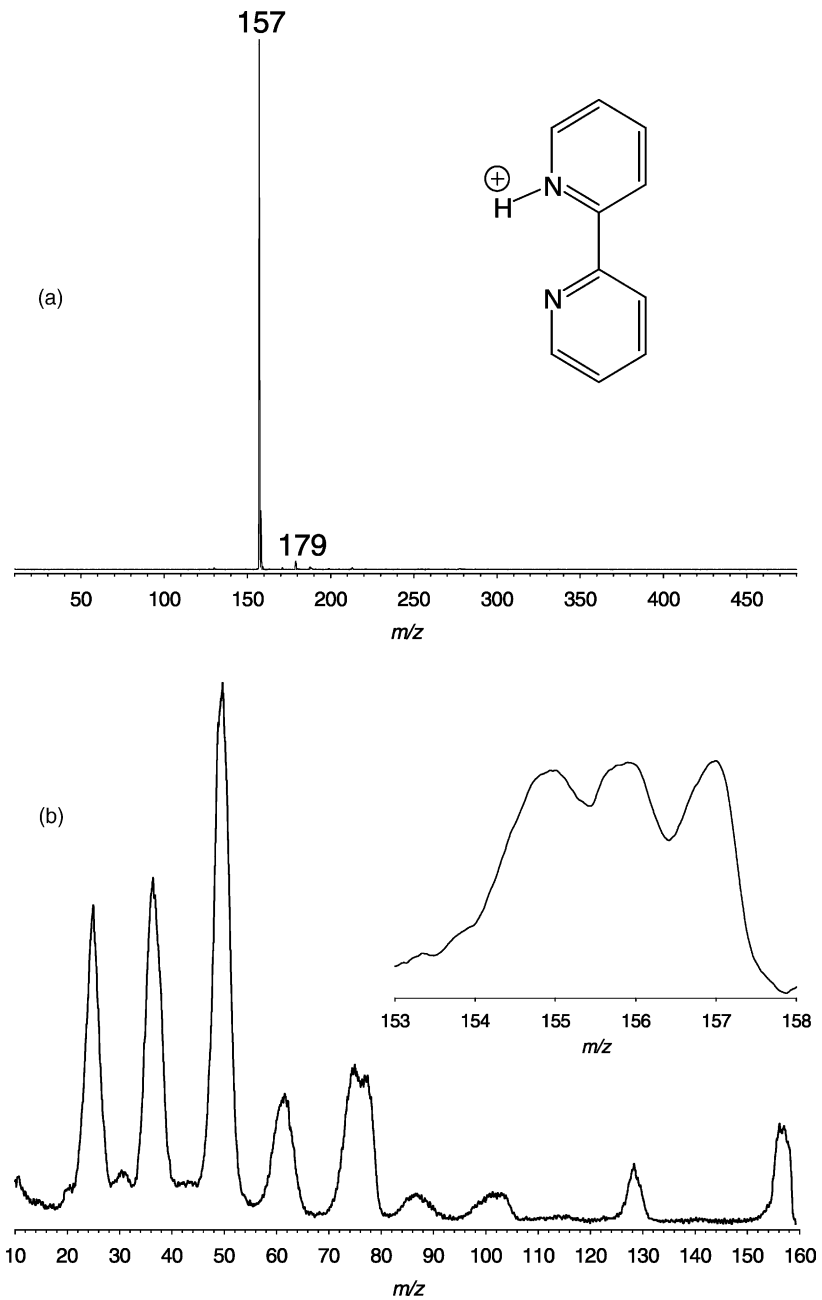

Fig. 8. (a) ESI mass spectrum of 2,2′-bipyridine. (b) $^+NR^+$ mass spectrum of [2,2′-bipyridine + H]$^+$ obtained as a kinetic energy scan.

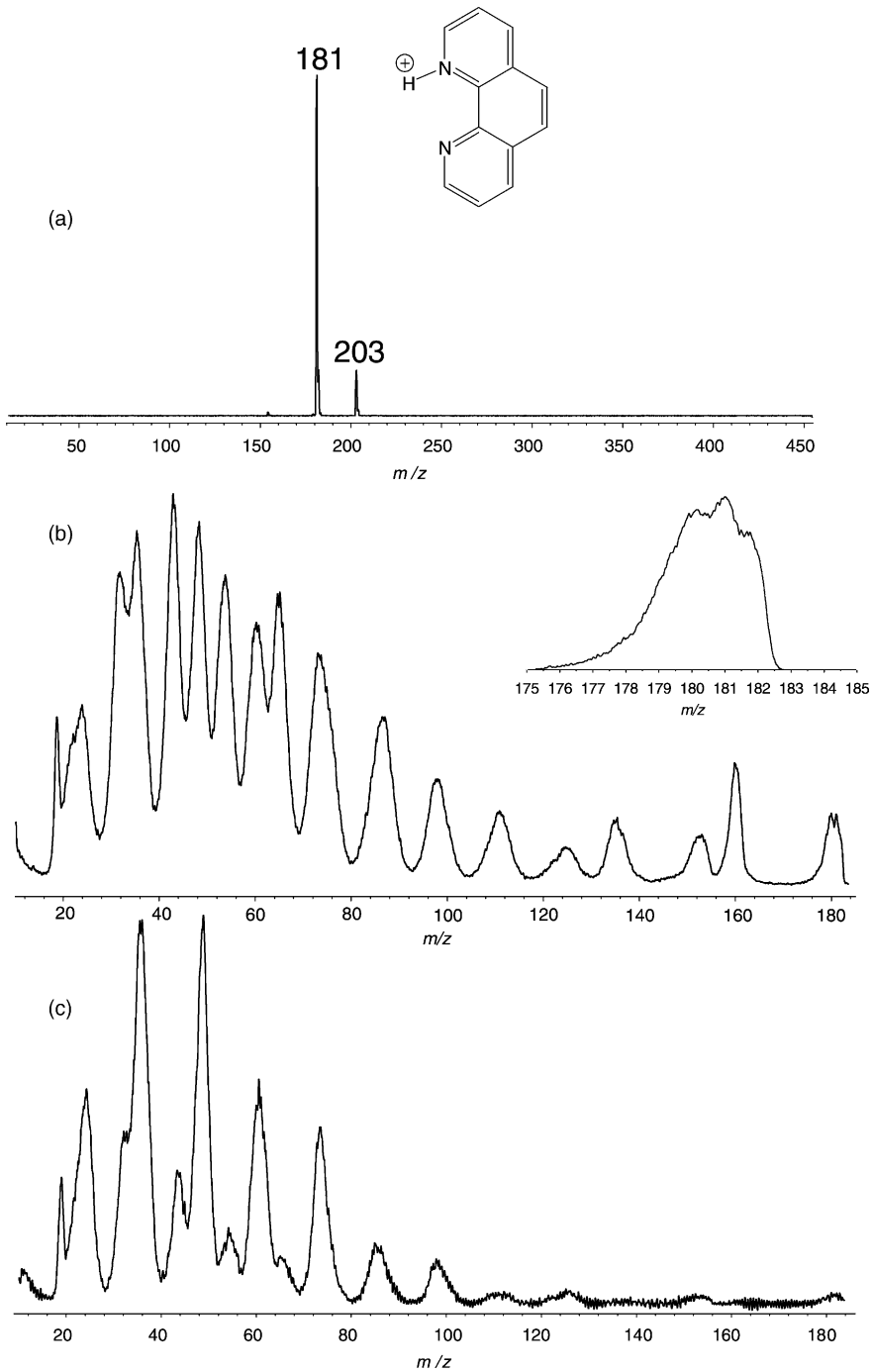

Fig. 9. (a) ESI mass spectrum of 1,10-phenanthroline. (b) $^{+}NR^{+}$ mass spectrum of [1,10-phenanthroline + H]$^{+}$ obtained as a kinetic energy scan. (c) $^{+}NR^{+}$ mass spectrum of [1,10-phenanthroline + H]$^{+}$ obtained as a linked kinetic energy/mass scan.

(C_2N), 28 (HCNH), and 27 (HCN) that correspond to ring-cleavage dissociations and formation of small fragments. The inset in Fig. 7b shows the survivor ion group of the $[A\text{-}d_3 + D]^+$ ion that was obtained by ESI ionization from a $CD_3OD + D_2O$ solution. Loss of both H (minor) and D (major) is observed that is likely to originate from the intermediate radical $[A\text{-}d_3 + D]^\bullet$ by analogy with dissociations of

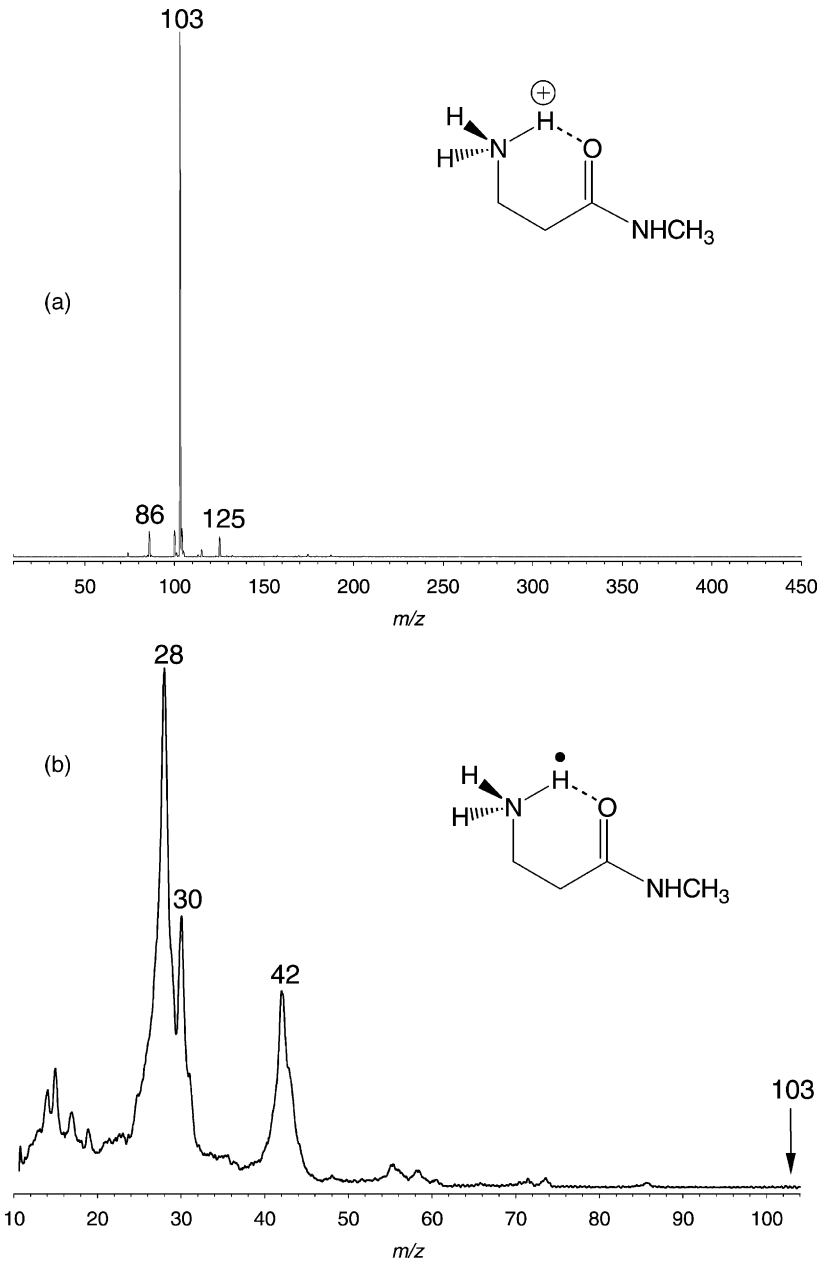

Fig. 10. (a) ESI mass spectrum of β-alanine-*N*-methyl amide. (b) $^+NR^+$ mass spectrum of $[H_3NCH_2CH_2CONHCH_3]^+$ obtained as a kinetic energy scan.

other nucleobase [28–30] and heterocyclic radicals [31–33].

ESI of 2,2′-bipyridine and 1,10-phenanthroline produces mainly the corresponding $[M+H]^+$ ions, as evidenced by the major peaks at *m/z* 157 (Fig. 8a) and *m/z* 181 (Fig. 9a), respectively. The main side products are the corresponding $[M + Na]^+$ ions at *m/z* 22 units higher. $^+NR^+$ of protonated 2,2′-bipyridine, monitored as a kinetic energy scan, yields a substantial peak of the survivor ion (Fig. 8b) that attests to the stability of the intermediate radical. Dissociation shows loss of one and two H atoms (Fig. 8b, inset), loss of HCN or CNH (*m/z* 130) in combination with H losses, loss of pyridine (*m/z* 79, 78), and ring-cleavage forming fragments at *m/z* 60–62, 48–52, 36–38, and 24–26. The individual species within each group are unresolved in the kinetic energy scans.

$^+NR^+$ of the $[M + H]^+$ and $[M + Na]^+$ ions produced by ESI of 1,10-phenanthroline shows contribution of dissociations originating from both species when the spectrum is obtained as a mass-unresolved kinetic energy scan (Fig. 9b). This is evidenced by the peak at an apparent *m/z* 160 which by kinetic energy corresponds to the dissociation $[M + Na]^\bullet \rightarrow M + Na^\bullet$. The product kinetic energy is $E_{kin}(M) = [180/(180 + 23)]E_0 = 0.887E_0$, corresponding to an apparent mass $m_{app} = 0.887 \times 181 = 160.5$ in the spectrum where the mass scale is calibrated for the $[M + H]^+$ ion at *m/z* 181. Scanning quadrupole II in a mass selective mode removes the *m/z* 160 peak because the M product from $[M + Na]^\bullet$ does not have a correct combination of mass and kinetic energy to be transmitted. Mass scanning the $^+NR^+$ spectrum of the $[M + H]^+$ ion (Fig. 9c) further results in the absence or substantially lowered intensity of peaks at apparent *m/z* values of 135, 65, 54, 44, 32, and 20 that correspond to fragments of *m/z* 151, 73, 61, 49, 36, and 23 from the sodiated $[M + Na]^\bullet$ radical. The fact that these appear at all in the Fig. 9c spectrum is due to the relatively low resolution of the energy filter which has a typical bandwidth of 40–50 eV [24]. This implies that neutralization–reionization mass spectra of ions produced less selectively by ESI should be acquired in the mass-scanned mode to avoid artifact peaks.

The ESI mass spectrum of β-alanine-*N*-methyl amide (Fig. 10a) shows a relatively clean formation of the corresponding $[M + H]^+$ ion at *m/z* 103, which is transmitted by the funnel lens. Minor contaminants in the ESI spectrum show peaks at *m/z* 125 $[M + Na]^+$ and 86 $[M + H - NH_3]^+$. The most stable structure of the $[M + H]^+$ ion has been elucidated by ab initio calculations [34] that showed preferential protonation on the amine group and stabilization of the ammonium cation by intramolecular hydrogen bonding to the amide carbonyl, as shown in Fig. 10a. $^+NR^+$ of this mixture gives rise to a kinetic energy spectrum (Fig. 10b) that does not display a survivor ion at *m/z* 103. Dissociation proceeds by loss of NH_3 (*m/z* 86 and 17), CH_3NH_2 (*m/z* 72 and 31), and also H. The primary product of loss of H does not give rise to a stable cation radical following reionization, but its formation can be inferred indirectly from the abundant $CH_2NH_2^+$ ion at *m/z* 30, which is a logical fragment from α-cleavage dissociation of the β-alanine-*N*-methyl amide cation radical. The radical dissociations are relevant as models for electron-capture dissociation of larger peptides that have been investigated computationally as reported elsewhere [34]. In an ongoing study, we are comparing the $^+NR^+$ mass spectra of cations produced by ESI and gas-phase chemical ionization.

5. Conclusions

ESI has been successfully coupled to a tandem mass spectrometer to allow for studies of transient neutral species produced by collisional neutralization. This first communication presents only $^+NR^+$ mass spectra obtained on precursor cations. However, the technique opens the field for the studies of anions produced by ESI of carboxylates, phosphates, and sulfates that are relevant to nucleotides, lipids, and modified peptides and carbohydrates. These experiments are underway. Future instrumentation developments will be aimed at increasing the ion currents transmitted by the ESI interface and improving the mass resolution in the neutralization–reionization mass spectra.

Acknowledgements

Support by the National Science Foundation (Grant CHE-0090930) is gratefully acknowledged. We also thank Drs. Hak-No Lee and W. Tim Elam for helpful discussions of the instrument design.

References

[1] M. Yamashita, J.B. Fenn, J. Phys. Chem. 88 (1984) 4451.
[2] J.B. Fenn, M. Mann, C.K. Meng, S.F. Wong, C.M. Whitehouse, Mass Spectrom. Rev. 9 (1990) 37.
[3] J.C. Poutsma, R.A. Seburg, L.J. Chyall, L.S. Sunderlin, B.T. Hill, J. Hu, R.R. Squires, Rapid Commun. Mass Spectrom. 11 (1997) 489.
[4] G. Koster, M. Soskin, M. Peres, C. Lifshitz, Int. J. Mass Spectrom. 179/180 (1998) 165.
[5] C.-F. Ding, X.-B. Wang, L.-S. Wang, J. Phys. Chem. A 102 (1998) 8633.
[6] T. Wyttenbach, P.R. Kemper, M.T. Bowers, Int. J. Mass Spectrom. 212 (2001) 13.
[7] C. Wesdemiotis, F.W. McLafferty, Chem. Rev. 87 (1987) 485.
[8] J.L. Holmes, Mass Spectrom. Rev. 8 (1989) 513.
[9] F. Tureček, Org. Mass Spectrom. 27 (1992) 1087.
[10] D.V. Zagorevski, J.L. Holmes, Mass Spectrom. Rev. 13 (1994) 133.
[11] N. Goldberg, H. Schwarz, Acc. Chem. Res. 27 (1994) 347.
[12] C.A. Schalley, G. Hornung, D. Schroder, H. Schwarz, Chem. Soc. Rev. 27 (1998) 91.
[13] D.V. Zagorevski, J.L. Holmes, Mass Spectrom. Rev. 18 (1999) 87.
[14] F. Tureček, Top. Curr. Chem. 225 (2003) 75.
[15] A.W. McMahon, S.K. Chowdhury, A.G. Harrison, Org. Mass Spectrom. 24 (1989) 620.
[16] M. Polášek, F. Tureček, J. Phys. Chem. A 105 (2001) 1371.
[17] (a) R. Feng, C. Wesdemiotis, M.A. Baldwin, F.W. McLafferty, Int. J. Mass Spectrom. Ion Processes 86 (1988) 95;
(b) F. Tureček, D.E. Drinkwater, A. Maquestiau, F.W. McLafferty, Org. Mass Spectrom. 24 (1989) 669.
[18] M. Sadílek, F. Tureček, J. Phys. Chem. 100 (1996) 9610.
[19] (a) D.W. Kuhns, T.B. Tran, S.A. Shaffer, F. Tureček, J. Phys. Chem. 98 (1994) 4845;
(b) D.W. Kuhns, F. Tureček, Org. Mass Spectrom. 29 (1994) 463.
[20] P.O. Danis, R. Feng, F.W. McLafferty, Anal. Chem. 58 (1986) 355.
[21] M.J. Polce, M.M. Cordero, C. Wesdemiotis, P.A. Bott, Int. J. Mass Spectrom. Ion Processes 113 (1992) 35.
[22] S. Beranová, C. Wesdemiotis, Int. J. Mass Spectrom. Ion Processes 134 (1994) 83.
[23] M. Peschke, A.T. Blades, P. Kebarle, J. Phys. Chem. A 102 (1998) 9978.
[24] F. Tureček, M. Gu, S.A. Shaffer, J. Am. Soc. Mass Spectrom. 3 (1992) 493.
[25] (a) S.A. Shaffer, K. Tang, G.A. Anderson, D.C. Prior, H.R. Udseth, R.D. Smith, Rapid Commun. Mass Spectrom. 11 (1997) 1813;
(b) S.A. Shaffer, D.C. Prior, G.A. Anderson, H.R. Udseth, R.D. Smith, Anal. Chem. 70 (1998) 4111;
(c) S.A. Shaffer, A.V. Tolmachev, D.C. Prior, G.A. Anderson, H.R. Udseth, R.D. Smith, Anal. Chem. 71 (1999) 2957.
[26] A.V. Tolmachev, T. Kim, H.R. Udseth, R.D. Smith, T.H. Bailey, J.H. Futrell, Int. J. Mass Spectrom. 203 (2000) 31.
[27] E.C. Lynn, M.-C. Chung, C.-C. Han, Rapid Commun. Mass Spectrom. 14 (2000) 2129.
[28] F. Tureček, J. Mass Spectrom. 33 (1998) 779.
[29] E.A. Syrstad, S. Vivekananda, F. Tureček, J. Phys. Chem. A 105 (2001) 8339.
[30] J.K. Wolken, F. Tureček, J. Phys. Chem. A 105 (2001) 8352.
[31] J.K. Wolken, F. Tureček, J. Am. Chem. Soc. 121 (1999) 6010.
[32] J.K. Wolken, F. Tureček, J. Phys. Chem. A 103 (1999) 6268.
[33] V.Q. Nguyen, F. Tureček, J. Am. Chem. Soc. 119 (1997) 2280.
[34] F. Tureček, E.A. Syrstad, J. Am. Chem. Soc. 125 (2003) 3353.